M. R. Alam (Corresponding Author), F. Bai, R. Yan, and T. K. Saha, "Classification and Visualization of Power Quality Disturbance-Events using Space Vector Ellipse in Complex Plane", IEEE Transactions on Power Delivery, July, 2020.
DOI: 10.1109/TPWRD.2020.3008003

Classification and Visualization of Power Quality Disturbance-Events using Space Vector Ellipse in Complex Plane

Mollah Rezaul Alam, *Member, IEEE*, Feifei Bai, *Member, IEEE*, Ruifeng Yan, *Member, IEEE* and Tapan Kumar Saha, *Fellow, IEEE*

***Abstract*—This article proposes a novel algorithm employing space vector ellipse (SVE) in a complex plane to classify and visualize power quality disturbance-events (PQDEs). In the proposed method, at first, the time-domain signal and a reference signal, which are separated by 90°, are mapped in a complex 2D coordinates. Thus, the tip of resultant rotating vector traces an ellipse, from which three parameters, namely, semi-major axis, semi-minor axis and inclination angle, are obtained. Then, the ellipse parameters are exploited to classify and visualize nine types of PQDEs, namely, voltage sag, swell, interruption, harmonic, sag-harmonic, swell-harmonic, notch, flicker and transient. To validate the practicability of the proposed approach, an extensive real-time simulation study is carried out on RTDS platform using a test microgrid network to generate a large number of PQDEs. The test events were successfully classified and visualized in complex plane. Moreover, the noisy and practical signals, recorded by IEEE 1159.2 Working Group, were successfully classified to demonstrate the effectiveness of the proposed method.**

***Index Terms*—Power quality disturbance-events, space vector ellipse, complex plane, classification, visualization.**

I. Introduction

POWER system may encounter various types of power quality disturbance-events (PQDEs), such as, voltage sag, voltage swell, transient, harmonics, notches, interruption, flicker, etc., which cause degradation of power quality (PQ) [1]. Switching of a large capacitor bank at the distribution network can trigger voltage swell. Transients may be observed during transformer energizing, switching of capacitor banks, etc. Arc furnaces may cause flickers; solid-state switching devices and non-linear loads may give rise to harmonic distortion [2]. If these PQDEs are not mitigated appropriately, malfunction or even permanent loss of equipment may lead to serious concern for both utilities and customers.

International standards, such as IEC 61000, IEEE 1159 and EN 50160, recommended a set of rules for the PQ limits; violating these PQ limits may cause the equipment to malfunction [1], [3]. The electricity network must be operated within the standard PQ limits (voltage, harmonic limit, etc.) in order to ensure safe and stable operation. To this end, the quality of power can be guaranteed if PQDEs are mitigated with proper controlling action. However, detection and recognition of PQDEs play a vital role to operate the controller efficiently. Therefore, automatic detection and classification of PQDEs are required to be devised.

Traditionally, root-mean-square (RMS) or half-cycle RMS values are used to classify sag, swell, interruption events; however, other PQDEs, such as notch, flicker, oscillatory transients could not be classified by RMS approach only. Hence, over the last few decades, various signal processing techniques, such as Fourier Transform (FT), Discrete Cosine Transform (DCT), Short-Time Fourier Transform (STFT), Hilbert-Huang Transform (HHT), Discrete Wavelet Transform (DWT), S-Transform (ST), etc., have been investigated to classify and characterize PQDEs [2], [4-14]. Fourier Transform (FT) is simple but fails to classify and characterize non-stationary PQ events [4]. With the introduction of Short-Time Fourier Transform (STFT), the problem is reported to be resolved; however, STFT fails to achieve standard resolution in time and frequency domain, consequently, performance is degraded [6]. Recently, the Discrete Wavelet Transform (DWT) has widely been adopted by many researchers across the world to detect and classify PQDEs [6-11]. However, noise in signals may deteriorate the performance of DWT [14]. S-transform (ST), on the other hand, is insensitive to noise and it shows better time-frequency resolution [14]. Features, extracted from most of these signal processing techniques, are fed into supervised or unsupervised classifiers, e.g., artificial neural network (ANN), probabilistic neural network (PNN), Decision Tree (DT), support vector machine (SVM), *k*-nearest neighbor (*k*-NN), etc., to identify the PQDEs [13-19]. Therefore, the substantial computational cost, which would come along these reported techniques, may fail to detect the power system disturbances in real time [19]. For example, power system electromagnetic phenomena, specifically, the transient and short duration RMS variations, which could be less than 1 cycle in duration [1], may not be detected and classified in real time due to the computational complexity of reported methods. Hence, a single methodological approach, which ensures accuracy, robustness, less complexity and low computational burden, is needed to be developed.

The authors are with the School of IT and Electrical Engineering, The University of Queensland, Brisbane, QLD 4072, Australia (email: mollahrezaul.alam@uq.edu.au; ruifeng@itee.uq.edu.au; f.bai@uq.edu.au; saha@itee.uq.edu.au)

In general, most of the conventional methods, as discussed in the literature, employed pattern recognition technique, which typically follows a five-step procedure [20]. The steps are: 1) pre-processing raw data, 2) patterns identification, 3) extraction of feature, 4) selection of decisive feature and 5) classification. To conduct these steps, these methods typically rely on training and testing framework, where the training step exploits a set of labelled events to yield a trained classifier with an optimal map between feature vectors and decision boundaries. The testing procedure takes the feature vector of an unlabeled event/sample as an input to the trained classifier and categorizes the true class of the unlabeled sample. Therefore, the detection and classification of PQDEs could be computationally expensive for these conventional methods. Moreover, visualization of PQDEs in real time could also increase the computational burden which might be a challenging task for the conventional methods. Unlike conventional methods, the proposed approach does not require any training procedure, and hence, it allows the flexibility for real time implementation of the proposed method to classify PQDEs along with their visualization.

In this article, a new approach for classification and visualization of PQDEs, namely, voltage sag, voltage swell, transient, harmonics, notches, interruption, flicker, is presented. The proposed approach transforms the PQ disturbance signals into space vector ellipse (SVE) in a complex plane; to this end, the disturbance signal and a reference signal are mapped in a complex 2D coordinates, which gives rise to an ellipse. The ellipse parameters, namely, semi-major axis (σ_{ma}), semi-minor axis (σ_{mi}) and inclination angle (ϕ), are exploited to develop an algorithm employed in classification and visualization of different PQDEs. Note that SVE has also been employed in [21-23] where 3-phase voltage signals are exploited in order to obtain the representation in the complex alpha-beta plane; whereas, in the proposed approach, instantaneous single-phase PQ signal and an artificial ideal reference signal are mapped on two orthogonal axes, which yields SVE to reflect the PQ disturbances through semi-major and semi-minor axes parameters. Moreover, the objective of [21-23] was to detect and classify balanced and unbalanced fault associated voltage sag and swell events; PQ disturbances, such as, notch flicker, interruption, transients were not considered in [21-23]. In contrast, the proposed algorithm detects, classifies and visualizes PQDEs in real-time by exploiting single-phase signals or exploiting each of the three-phase signals separately. Besides, the proposed approach offers the following advantages over other methods: 1) easy to implement, 2) less computational burden, 3) provides a simple platform to visualize the events in real-time, 4) substantial classification accuracy which is validated by real data.

The remainder of the paper is organized as follows. Section II presents the analytical formulation of space vector ellipse and its associated parameters; time-domain representation of PQDEs and their visualization in a complex plane is also presented. The proposed algorithm is outlined in Section III. Section IV validates the proposed method, which is demonstrated through the classification accuracy with real data of IEEE 1159.2 working group as well as with the data generated from real-time simulated PQDEs on RTDS platform. Final conclusion is discussed in Section V.

II. Space Vector Ellipse and its Visualization during Power Quality Disturbances

This Section firstly presents the power quality disturbance-events (PQDEs) and their representative equations. Then, analytical formulation of space vector ellipse (SVE) and its associated parameters are described. Lastly, the visualization of SVEs during PQDEs is outlined.

A. Representative Equations of Power Quality Disturbance-Events

Table I shows the representative equations for PQDEs, namely, voltage sag, voltage swell, interruption, harmonic, sag-harmonic, swell-harmonic, oscillatory transient, notch, and flicker. The events are expressed analytically following the definitions presented in IEEE Standard 1159-2009 [1]. For example, according to [1], voltage swell is defined as an increase in voltage/current (RMS) at power system frequency to a typical value in between 1.1-1.8 pu for durations from 0.5 cycles to 1 min. Hence, in Table I, the expression of voltage swell includes the pu values of the signals within 1.1-1.8 for a typical duration of 1 cycle to 9 cycles. Likewise, other PQ disturbance signals are expressed, see Table I for further details.

TABLE I
Representative Equations for Power Quality Disturbance-Events

PQDEs	Equations	Range of variables
Normal	$s(t) = \sin(\omega_n t)$	$\omega_n = 2\pi f_n$, where f_n is fundamental frequency of power system
Sag	$s(t) = [1 - \alpha(u(t-t_1) - u(t-t_2))]\sin(\omega_n t)$	$0.1 \le \alpha \le 0.9,\ T \le t_2 - t_1 \le 9T$
Swell	$s(t) = [1 + \alpha(u(t-t_1) - u(t-t_2))]\sin(\omega_n t)$	$0.1 \le \alpha \le 0.8,\ T \le t_2 - t_1 \le 9T$
Interruption	$s(t) = [1 - \alpha(u(t-t_1) - u(t-t_2))]\sin(\omega_n t)$	$0.9 \le \alpha \le 1,\ T \le t_2 - t_1 \le 9T$
Harmonic	$s(t) = \alpha_1 \sin(\omega_n t) + \alpha_3 \sin(3\omega_n t) + \alpha_5 \sin(5\omega_n t) + \alpha_7 \sin(7\omega_n t)$	$0.05 \le \alpha_3, \alpha_5, \alpha_7 \le 0.15, \sum(\alpha_i)^2 = 1$
Sag-harmonic	$s(t) = [1 - \alpha(u(t-t_1) - u(t-t_2))][\alpha_1 \sin(\omega_n t) + \alpha_3 \sin(3\omega_n t) + \alpha_5 \sin(5\omega_n t)]$	$0.1 \le \alpha \le 0.9,\ T \le t_2 - t_1 \le 9T, 0.05 \le \alpha_3, \alpha_5 \le 0.15, \sum(\alpha_i)^2 = 1$
Swell-harmonic	$s(t) = [1 + \alpha(u(t-t_1) - u(t-t_2))][\alpha_1 \sin(\omega_n t) + \alpha_3 \sin(3\omega_n t) + \alpha_5 \sin(5\omega_n t)]$	$0.1 \le \alpha \le 0.8,\ T \le t_2 - t_1 \le 9T, 0.05 \le \alpha_3, \alpha_5 \le 0.15, \sum(\alpha_i)^2 = 1$
Notch	$s(t) = \sin(\omega_n t) - \text{sign}(\sin(\omega_n t)) \times \{\sum_{n=0}^{9} \mathcal{L} \times [u(t - (t_1 + 0.02n)) - u(t - (t_2 + 0.02n))]\}$	$0.1 \le \mathcal{L} \le 0.4, t_1 \ge 0, t_2 \le 5T,\ 0.01T \le t_2 - t_1 \le 0.05T$
Flicker	$s(t) = [1 + \alpha \sin(2\pi\gamma t)]\sin(\omega_n t)$	$0.1 \le \alpha \le 0.2,$ $5\text{ Hz} \le \gamma \le 20\text{ Hz}$
Oscillatory Transient	$s(t) = \sin(\omega_n t) + \alpha e^{\frac{-(t-t_1)}{\tau}}(u(t-t_1) - u(t-t_2))\sin(2\pi f_m t)$	$0.1 \le \alpha \le 0.8,\ 0.5T \le t_2 - t_1 \le 3T, 300\text{ Hz} \le f_m \le 900\text{ Hz}, 8\,ms \le \tau \le 40\,ms$

B. Analytical Formulation of Space Vector Ellipse

The first harmonic of the signals associated with the PQDEs, can be expressed as sinusoidal quantities in time-domain before, during and after the disturbances. Following the assumption and then, employing Euler's rule, the signals can be expressed as the sum of two phasors rotating in the opposite direction with angular frequency ω, which is given by

$$s(t) = |\boldsymbol{S}| \sin(\omega t) = \frac{|\boldsymbol{S}|}{2j}(e^{j\omega t} - e^{-j\omega t}) \quad (1)$$

A reference signal, $s_{ref}(t)$, having ideal magnitude, angular frequency ω and phase-angle difference of 90° with $s(t)$, can be

presented as

$$s_{ref}(t) = |\boldsymbol{S}_{ref}| \sin\left(\omega t + \frac{\pi}{2}\right) = \frac{|\boldsymbol{S}_{ref}|}{2j}\left(e^{j\left(\omega t+\frac{\pi}{2}\right)} - e^{-j\left(\omega t+\frac{\pi}{2}\right)}\right) \quad (2)$$

Now, from (1) and (2), the space vector, $\vec{\boldsymbol{R}}(t)$, is formed as

$$\vec{\boldsymbol{R}}(t) = \begin{bmatrix}1 & e^{\frac{j\pi}{2}}\end{bmatrix}\begin{bmatrix}s(t)\\ s_{ref}(t)\end{bmatrix} \quad (3)$$

Equation (3) basically transforms the signal $s(t)$ in space vector domain, where the variation of $s(t)$ with respect to ideal reference signal $s_{ref}(t)$ is reflected in the tip of resultant rotating space vector $\vec{\boldsymbol{R}}(t)$. Now, using (1)-(3), the space vector, $\vec{\boldsymbol{R}}(t)$, can be simplified as

$$\vec{\boldsymbol{R}}(t) = \left(\frac{|\boldsymbol{S}|}{2}e^{-\frac{j\pi}{2}} + \frac{|\boldsymbol{S}_{ref}|}{2}e^{\frac{j\pi}{2}}\right)e^{j\omega t} + \left(\frac{|\boldsymbol{S}|}{2}e^{\frac{j\pi}{2}} - \frac{|\boldsymbol{S}_{ref}|}{2}e^{-\frac{j\pi}{2}}\right)e^{-j\omega t} \quad (4)$$

Equation (4) is equivalent to the ellipse, which is originated from the sum of negative and positive angular frequency phasors [24], i.e.,

$$\vec{\boldsymbol{R}}(t) = \boldsymbol{R}^{+}e^{j\omega t} + \boldsymbol{R}^{-}e^{-j\omega t} \quad (5)$$

where $\boldsymbol{R}^{+} = |\boldsymbol{R}^{+}|e^{j\phi^{+}}$ and $\boldsymbol{R}^{-} = |\boldsymbol{R}^{-}|e^{j\phi^{-}}$; semi-major axis ($\sigma_{ma}$), semi-minor axis ($\sigma_{mi}$) and inclination angle (ϕ) are given by

$$\sigma_{ma} = \left||\boldsymbol{R}^{+}| + |\boldsymbol{R}^{-}|\right| \quad (6)$$

$$\sigma_{mi} = \left||\boldsymbol{R}^{+}| - |\boldsymbol{R}^{-}|\right| \quad (7)$$

$$\phi = (\phi^{+} - \phi^{-}) \quad (8)$$

Thus, employing space vector transformation on the signals of PQDEs, three SVE parameters, namely, semi-major axis, semi-minor axis and inclination angle, are deduced. In summary, by mapping the PQDE signal and an artificial ideal reference signal on two orthogonal axes, a space vector ellipse (SVE) is obtained where PQ disturbances are reflected in the semi-major and semi-minor axes parameters.

C. Visualization of Space Vector Ellipse during Power Quality Disturbance-Events

In this article, space vector ellipse (SVE) is obtained from the space vector transformation of the signals corresponding to PQDEs. To illustrate the visualization of the SVE, firstly, the mapping of $s(t)$ and $s_{ref}(t)$ is conducted on the real and imaginary axis, respectively. Then, the resultant of these time-domain signals produces a rotating space vector, $\vec{\boldsymbol{R}}(t)$, whose tip traces an ellipse in the complex plane as shown in Fig. 1(a). Fig. 1(a) is obtained from (1)-(8) considering the reference signal as a sinusoid with $|\boldsymbol{S}_{ref}| = 1$ pu, $s(t)$ as a normal signal, which is not affected by PQ disturbances. Thus, SVE and its associated parameters are achieved, see Fig. 1(a).

The visualization of PQDEs in space vector domain is illustrated in Fig. 1(b) and Fig. 2. In Fig. 1(b), the PQDEs, which are greatly influenced by the deviation of voltage magnitude, for instance, voltage sag, swell, interruptions, are demonstrated as a series of SVEs. Note that these series of SVEs are obtained from cycle-by-cycle space vector transformation of the PQ disturbance signals. Complying with the IEEE 1159-2009 standard, voltage sag, swell, interruption and normal signal zone are clearly highlighted in Fig. 1(b).

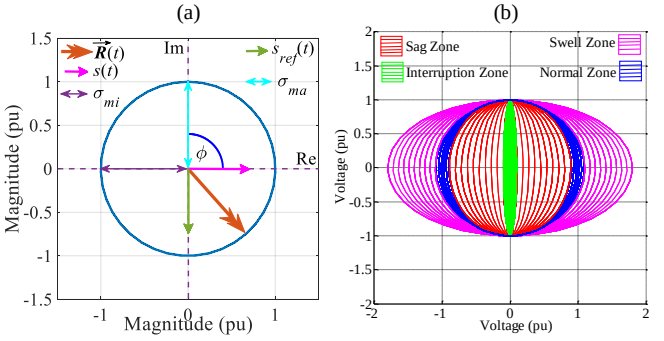

Fig. 1. (a) Formation of space vector ellipse (SVE) from the tip of resultant rotating vector, $\vec{\boldsymbol{R}}(t)$ and SVE parameters, semi-major axis (σ_{ma}), semi-minor axis (σ_{mi}), inclination angle (ϕ), in a complex plane; (b) shape of space vector ellipses (SVEs) during normal condition, voltage sag, swell, interruption events and their specified zones.

Unlike Fig. 1(b), the SVEs of Fig. 2 exhibit different shape for the PQDEs, which are greatly influenced by high and low order harmonics or inter-harmonics. Voltage flicker, notch, transient, harmonic, sag-harmonic and swell-harmonic belong to such PQDEs. Note that for each event, PQ signals with 1 sec duration is passed through the SVE transformation. For notch signal, a regular pattern of spike in the SVE is observed; for flicker signal, several cycles of sags and swells are found within 1 sec. Transient is exhibited by the irregular shapes, whereas a wave-like pattern is observed for harmonic affected PQDE. Sag-harmonic and swell-harmonic falls inside the sag and swell zone, respectively, along with harmonic pattern; see Fig. 2 for illustration.

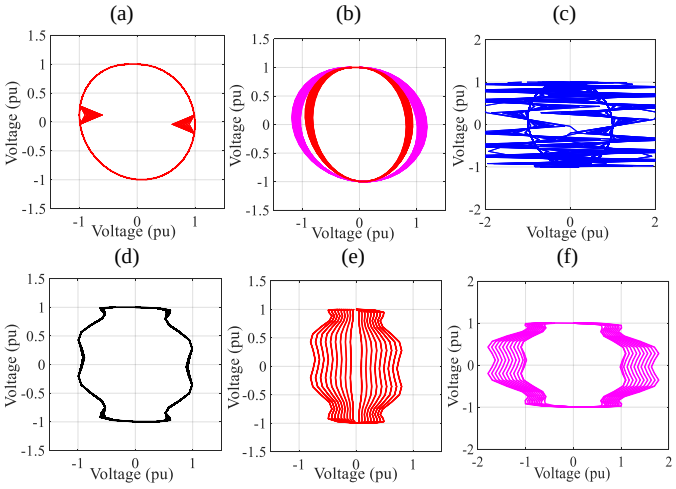

Fig. 2. Shape of space vector ellipses (SVEs) during power quality disturbance-events (PQDEs): (a) notch, (b) flicker, (c) oscillatory transient, (d) harmonic, (e) sag-harmonic, and (f) swell-harmonic.

III. Proposed Approach for PQ Disturbance-Events Classification

The proposed algorithm takes the PQ disturbance signals as input and classifies them into different PQDEs. To this end, real-time classification of the signals is conducted in two stages. Firstly, sag, swell, sag-harmonic, swell-harmonic, interruption events are classified on a cycle-by-cycle basis employing SVE transformation. Secondly, the same signals within 10-cycle data-window are classified employing FFT (Fast Fourier Transform) and SVE transformation followed by a few decision-

making rules. Thus, normal event, notch, transient, flicker and harmonics are distinguished.

Fig. 3 illustrates the proposed algorithm in two stages. At the first stage, sag, swell, sag-harmonic, swell-harmonic and interruption events are classified. According to IEEE 1159-2009 standard, sag, swell and interruption events are defined in terms of a typical range of voltage magnitude and duration of 0.5 cycle to 1 min. Therefore, in our method, cycle-by-cycle classification is conducted by employing SVE transformation on voltage signal (in pu), which yields semi-major (σ_{ma}) and semi-minor (σ_{mi}) axes. Complying with the standard, if σ_{mi} of less than 0.1 is found, then the event is classified as an interruption. Similarly, if σ_{mi} lies within the range of 0.1-0.9, then sag event is detected; for $\sigma_{ma} \geq 1.1$, swell event is identified. Total harmonic distortion of voltage (THD_v) quantifies the amount of harmonic component in the signal. FFT is applied to compute THD_v and if it exceeds the maximum PQ limit of 5%, then the signal is classified as harmonic affected PQDE. If both sag and harmonic is present in the signal, then, the sag-harmonic event is classified. Similarly, the simultaneous existence of swell and harmonic distinguishes the event as swell-harmonic. Note that estimation of THD_v through FFT would not be an issue in terms of computational speed of the proposed method. Since, according to [25], the computational time for 400-point (random or deterministic input sequence) FFT is 0.035 ms; therefore, for a time-length of 20 ms per cycle (50 Hz system), cycle-by-cycle classification is possible in real-time using the proposed algorithm.

Classification of notch, flicker, oscillatory transient and harmonic events are carried out in the second stage. These events are characterized by the harmonic and interharmonic components of the fundamental frequency of the power system. Therefore, in the proposed approach, to classify these events, firstly, FFT is applied and then, the magnitudes of harmonic and interharmonic components are associated with sinusoids prior to transforming them into SVE domain. For example, if FFT decomposes a signal in frequency domain into 3rd, 5th, and 7th order harmonics with the amplitude of 0.1, 0.033 and 0.011 pu, respectively, then, three signals, $0.1\sin(\omega t)$, $0.033\sin(\omega t)$ and $0.011\sin(\omega t)$, are transformed separately in the complex SVE domain. Note that during SVE transformation of the three signals, $\sin(\omega t + \pi/2)$ is considered as a reference signal. Thus, semi-minor and semi-major axes are achieved, which are denoted as σ_{mi_f} and σ_{ma_f}, respectively; a subscript *f* is added in the symbols for distinguishing them from the σ_{mi} and σ_{ma} denoted in the first stage.

As shown in Fig. 3, a sliding data-window of 10-cycle typical length is used in the second stage, wherein PQ disturbance signals is processed. Thus, the SVE parameters, which are needed for classification, are acquired. If SVE transformation for the maximum amplitude of higher order harmonics results in σ_{mi_f} of 0.05-0.10, then, the transient event is identified. Note that in this case, typical value of higher order harmonics is considered above 50th order (i.e., above 50×50=2500 Hz for a power system with 50 Hz nominal frequency), which is in compliant with the definition of transient event recommended in IEEE 1159-2009 standard. Complying with the definition as advised in IEEE standard, a disturbance is identified as notch if $0.01 \leq \sigma_{mi\_f} < 0.05$ for 2nd to higher order harmonics. Flicker is reflected in the signal with the signification variation (rise and fall) in amplitude as well as with the presence of interharmonic component. Therefore, in the proposed approach, two conditions are imposed to distinguish flicker events, which include: 1) time-derivative of σ_{mi_f}, i.e., $d\sigma_{mi\_f}/dt$, should be greater than 0.05 for 3 cycles or more and 2) Maximum value of σ_{mi_f} for interharmonic components should lie within 0.05-0.1, where frequencies of interharmonic components are less than fundamental frequency of power system. Lastly, FFT is applied on a 10-cycle signal to compute THD_v and if it exceeds the maximum PQ limit of 5%, then the signal is classified as harmonic affected PQDE. Note that the proposed approach is applicable for single-phase as well as three-phase signals; however, for three-phase signals, each phase has to be considered separately and passed through the algorithm shown in Fig. 3.

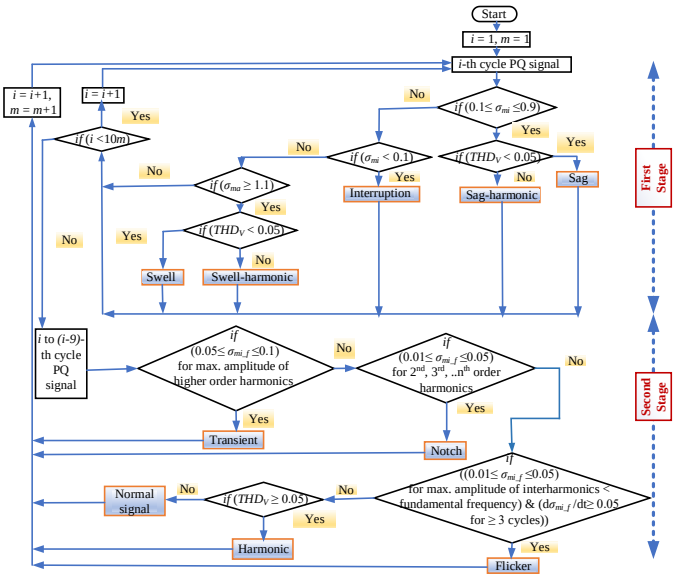

Fig. 3. Flowchart illustrating the classification algorithm for PQ disturbance signals.

IV. Validation of Proposed Approach and Test Results

This Section presents the validation of proposed approach, which is conducted through the classification performance of PQ disturbance signals under different test environment. Subsection IV-A demonstrates the test results with synthetic data. Subsection IV-B validates the proposed method by exhibiting its performance with real data of IEEE 1159.2 working group (WG) and DOE/EPRI. Finally, in subsection IV-C, the PQ disturbance signals, generated from real-time simulation of a microgrid test system on RTDS platform, are tested and the results are detailed.

A. Validation with synthetic PQ disturbance signals

A set of synthetic data representing a total of 1800 PQ disturbance signals associated with nine PQDEs, which include voltage sag, swell, harmonic, interruption, sag-harmonic, swell-harmonic, flicker, notch, and transient, are tested to validate the proposed approach. The representative equations of Table I are exploited to generate the test synthetic data. To this end, the variables shown in 3rd column of Table I are varied within their

specified range. Thus, a total of 200 PQ disturbance signals for each PQDE are produced. For example, exploiting the representative sag equation of Table I, 200 sag events are produced

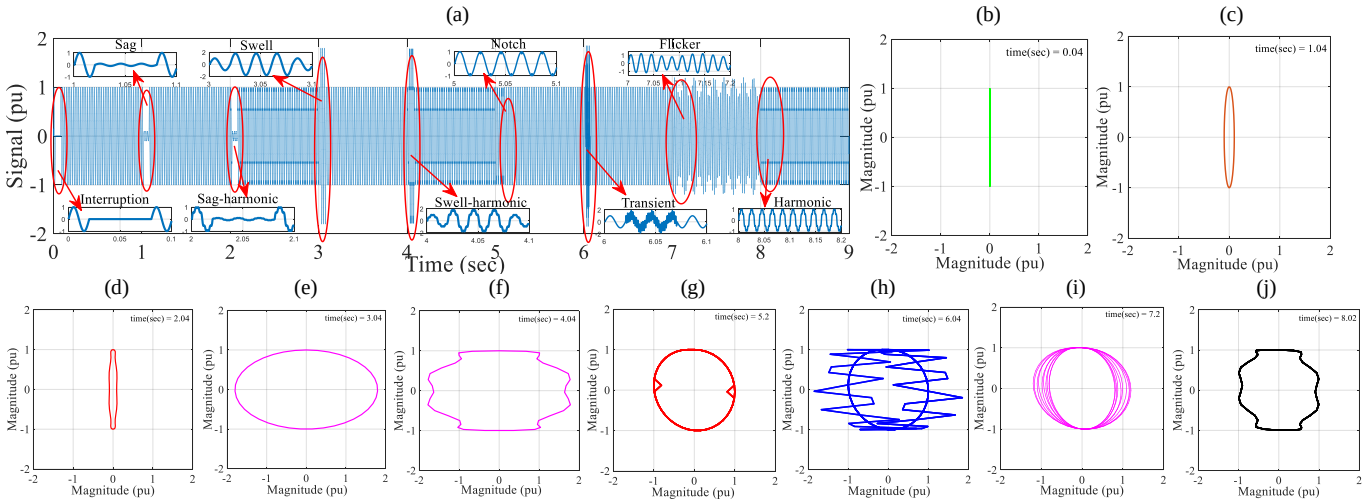

Fig. 4. (a) PQ disturbance signal; classified space- vector ellipses (SVEs) and their visualization with detection time (sec) for (b) interruption, (c) sag, (d) sag-harmonic, (e) swell, (f) swell-harmonic, (g) notch, (h) transient, (i) flicker and (j) harmonic events.

by varying α from 0.1 to 0.9 and sag-duration between 1 to 9 cycle. Similarly, other PQ disturbance signals are generated.

Using the expressions illustrated in Table I, a simple script is executed to produce the set of synthetic data containing 1800 PQ disturbance signals, where the duration of each signal is 1 sec. Then, the signals are passed through the proposed algorithm to demonstrate the visualization and classification performance. Firstly, the performance is assessed for an example PQ signal. Then, the classification performance is evaluated for the set of synthetic data with and without noise of different level.

The classification and visualization performance are demonstrated by testing an example PQ signal of 9 sec length; the example signal comprises of nine PQDEs with each having 1 sec duration, see Fig. 4(a) for illustration. Note that, within 1 sec duration of each PQDE, length of affected zone varies from a few cycles to 1 sec. For instance, in the test signal, voltage sag begins at 1.02 sec and ends at 1.08 sec, indicating sag duration of 3 cycles for 50 Hz system. Harmonic affected signal, with 1 sec length, starts at 8 sec and ends at 9 sec.

The proposed algorithm classifies successfully the example test signal and the results can be seen in Figs. 4(b)-(j). As illustrated in the flowchart of Fig. 3, classification is conducted within sliding data-window of 1 cycle and 10-cycle long. Voltage sag, swell, interruption, sag-harmonic and swell-harmonic are classified within 1-cycle data-window, whereas transient, notch, flicker and harmonic events are classified within 10-cycle data-window. Hence, PQDEs are successfully detected within 1 to 10 cycles of events' inception timestamp. Figs. 4(b)-(j) reveals the classification results for example test signal along with the detection timestamp after events' inception. Voltage sag, swell, interruption, sag-harmonic, transient, notch, harmonic and swell-harmonic events are classified and detected after 1-2 cycle of their respective inception time, see Figs. 4(b)-(j). For example, voltage swell incepts at 3.02 sec and the event is classified as well as detected at 3.04 sec, see Fig. 4(e). Moreover, real-time classification of the example PQDEs is demonstrated through a video, which can be seen from the link below: https://drive.google.com/file/d/1tO-zkKxVv4UvqY_X_7y73Gr3XP0M0T15D/view?usp=sharing

Note that in this study, 40 signal-samples per cycle is exploited, i.e., the sampling frequency (or sampling rate) of 2 kHz is used for 50 Hz signal. However, for real-time visualization of PQ disturbance events, 2 kHz is a typical sampling rate, which could be adjusted (increased/decreased) realistically depending on the computational capacity of the processor.

Table II illustrates the detailed classification performance of the proposed approach. A total of 1800 PQ disturbance signals representing nine PQDEs are classified with 100% detection rate. However, to test the robustness of the proposed approach under noisy environment, the PQ signals are mixed with SNR of 10 dB, 20 dB and 30 dB. The performance is marginally affected with the addition of noise, where detection rate of 98% and above is achieved for all test cases. The most conservative results are found for transient events with SNR of 10 dB. As shown in Table II, even for the most conservative case, 98% detection rate is found, which is considerably acceptable.

TABLE II
Classification Results of Proposed Method with Synthetic data of PQ Disturbance-Events (PQDEs)

PQDEs	No. of events	Detection Rate for PQ disturbance signals			
		Noise free	SNR 30 dB	SNR 20 dB	SNR 10 dB
Sag	200	100%	100%	100%	100%
Swell	200	100%	100%	99%	99%
Interruption	200	100%	100%	100%	100%
Harmonic	200	100%	99.5%	99%	98.5%
Sag-harmonic	200	100%	99%	98.5%	98.5%
Swell-harmonic	200	100%	98.5%	98.5%	98.5%
Notch	200	100%	99%	100%	99%
Flicker	200	100%	99.5%	100%	99%
Oscillatory Transient	200	100%	99%	99%	98%

The frequency of practical power system may fluctuate during disturbances. Hence, to test the efficacy of proposed method under frequency deviation, the fundamental frequency of synthetic PQ signals (shown in Table I) are varied within a typical range of 47-52 Hz, and then, different power quality disturbance events (PQDEs) are classified by proposed method. Table

III shows the successful classification of such PQDEs with negligible compromise in detection rate.

TABLE III
Classification Results of Proposed Method using Synthetic data of PQ Disturbance-Events (PQDEs) with variation in Fundamental frequency

PQDEs	No. of events	Detection Rate for PQ disturbance signals with variation in frequency		
		47-48 Hz	49-50 Hz	51-52 Hz
Sag	200	100%	100%	100%
Swell	200	100%	100%	99%
Interruption	200	100%	100%	100%
Harmonic	200	99%	99%	98.5%
Sag-harmonic	200	98.5%	99%	99%
Swell-harmonic	200	98.5%	99%	98%
Notch	200	99.5%	99.5%	99.5%
Flicker	200	99%	99.5%	99.5%
Oscillatory Transient	200	99%	99%	99.5%

The detection rate of the proposed method is compared with a few methods reported in the literature. As such, the methods proposed in [26-29] are accounted for the comparative study. In [26-29], feedforward neural network and adaptive linear network [26], S-transform and fuzzy decision tree [27], S-transform and Dynamics [28], and discrete wavelet transform and wavelet networks [29] are used to detect and classify PQ disturbance signals. The classification results are tabulated in Table IV which exhibits better performance of the proposed method as compared to other methods. Moreover, the reported methods in [26-29] require training and testing steps, whereas the proposed method is free from such time-consuming steps.

TABLE IV
Comparative Performance Study of Proposed Method with other Methods for Detection of PQDEs

PQDEs	Detection Rate for PQ disturbance signals				
	Method in [26]	Method in [27]	Method in [28]	Method in [29]	Proposed Method (SNR 30 dB)
Sag	100%	99%	97.33%	97.33%	100%
Swell	100%	98%	98.66%	98.67%	100%
Interruption	100%	96%	96.99%	98%	100%
Harmonic	98%	99%	100%	99.33%	99.5%
Sag-harmonic	98%	97%	-	98.18%	99%
Swell-harmonic	97%	98%	96%	98.18%	98.5%
Notch	97%	98%	96%	97.33%	99%
Flicker	94%	96%	-	98.67%	99.5%
Oscillatory Transient	98%	99%	94	98.67%	99%

B. Validation with real PQ disturbance signals

IEEE 1159.2 working group (WG) recorded several test waveforms in [30]; the waveforms were collected during different PQ disturbance events, such as voltage sag, swell, harmonic, interruption, etc. In this subsection, the proposed approach is validated by demonstrating the successful classification of PQ signals associated with these real PQDEs.

Table V shows the classification results with the test waveforms, namely, wave3, wave6, wave8, etc. Note that for validation purpose, one of the three-phase voltages of these waveforms are used. However, our method can take input from all three-phases separately and classify them successfully. In this study, frequency of first harmonic is obtained as 60 Hz, since fundamental frequency of all recorded waveforms was 60 Hz. From the SVE parameters, semi-major axis (σ_{ma}) and semi-minor axis (σ_{mi}), voltage sag, and interruption events are successfully classified and detected. The results are shown in Table V for waves 3, 4, 6a, and 9. In Table V, classified window includes the PQ signals with events' inception timestamp, whereas detection time indicates the successful detection of events within 1 cycle (0.0167 s for 60 Hz system) of their inception time. In addition, the waveforms are decomposed by FFT to extract the harmonic and interharmonic components, which are required for the detection of harmonic, notch, transient and flicker events. Computing the harmonic and interharmonic components and then, following a few decision-making rules shown in Fig. 3, these PQDEs are classified and detected. Thus, sag-harmonic event is detected for waves 5, 7, 8, 13, swell-harmonic for waves 14a, 14c, and transient event is detected for wave 15. In order to conduct visual representation of the disturbance events, wave 13 is taken as an example, see Fig. 5 for illustration. In Fig. 5(b), the space vector ellipse (SVE) is obtained by processing one-cycle signal within classified window which includes the inception of events, see Fig. 5(a) for details. The SVE for sag-harmonic event is shown in Fig. 5(b). Thus, through our approach, the service of visual observation along with successful classification of PQDEs is achieved.

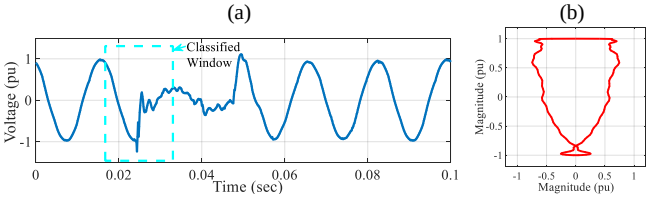

Fig. 5. (a) Voltage signal of wave 13, (b) Shape of SVE for sag-harmonic event detected within "classified window" enclosing 2nd cycle of wave 13.

TABLE V
Classification Results of Proposed Approach using IEEE 1159.2 WG data

Waveforms	SVE parameters		Classified window	Detection time (sec)	Classified PQDEs
	Semi-minor axis (σ_{mi})	Semi-major axis (σ_{ma})			
wave 3	0.5827	1.0038	1st cycle	0.0167	Sag
wave 4	0.5771	1.0038	1st cycle	0.0167	Sag
wave 5	0.4784	1.0038	2nd cycle	0.0167	Sag-harmonic
wave 6a	0.6317	1.0038	2nd cycle	0.0167	Sag
wave 7	0.2366	1.0038	2nd cycle	0.0167	Sag-harmonic
wave 8	0.1626	1.0038	1st cycle	0.0167	Sag-harmonic
wave 9	0.0774	1.0038	1st cycle	0.0167	Interruption
wave 13	0.5815	1.0038	2nd cycle	0.015	Sag-harmonic
wave 14a	1.0038	1.1027	1st cycle	0.0167	Swell-harmonic
wave 14c	1.0038	1.1011	1st cycle	0.0167	Swell-harmonic
wave 15	-	-	4th cycle	0.0167	Transient

Real data, which are associated with several PQ disturbance events, are collected from the national database repository of DOE/EPRI [31] and the proposed method is validated. The results are presented in Table VI. Note that the PQ signals of Table VI are classified using a sliding data-window in real-time.

However, the classification results within one classified window, i.e., the data-window which incorporates the inception timestamp, is tabulated. Semi-major and semi-minor axis parameters allow the signals 2831, 3235 and 3260 to be successfully classified as sag. Moreover, the events are detected within 1 cycle, i.e., 0.0167 s of events' inception.

TABLE VI
Classification Results of Proposed Approach using EPRI data

Signals	SVE parameters		Classified window	Detection time (sec)	Classified PQDEs
	Semi-minor axis (σ_{mi})	Semi-major axis (σ_{ma})			
2797	0.7002	1.0038	1st cycle	0.0167	Sag-harmonic
2831	0.8525	1.0038	2nd cycle	0.015	Sag
2911	1.0038	1.1	1st cycle	0.0167	Swell-harmonic
2948	0.6122	1.0038	2nd cycle	0.0167	Sag-harmonic
3235	0.7943	1.0038	2nd cycle	0.0167	Sag
3460	0.6544	1.0038	2nd cycle	0.0167	Sag

C. Test Results on Real-Time Digital Simulator (RTDS) Platform

As stated earlier, the proposed algorithm follows two-stage classification approach. The first stage classifies five PQDEs, namely, sag, swell, interruption, sag-harmonic, swell-harmonic, by conducting cycle-by-cycle classification with computational processing time <15 ms for each cycle; this computational time is less than the 1-cycle time-length of 50 Hz signal (which is 20 ms). The second stage classifies four PQDEs, namely, notch, flicker, oscillatory transients and harmonic events, within 10 cycle data-window of PQ signals with computational processing time <100 ms, which is substantially less than 10-cycle time-length of 50 Hz signal (i.e., 200 ms). Therefore, the computational speed of the proposed method is fast enough to conduct the respective PQ classification task before receiving the next data-window in real-time, which makes the approach applicable for classification and visualization of PQDEs in real-time. These computational processing times are obtained by executing the coded algorithm in MATLAB software (version 9.2 R2017a) hosted in a computer with the specifications: intel®corei7, CPU 1.9 GHz, RAM 16 GB.

Now, to demonstrate the applicability of the proposed method in real-time, this subsection demonstrates the validation of proposed approach through real-time (RT) simulation study. To this end, a test network is modelled in RSCAD software and simulated in RTDS hardware. MATLAB-RSCAD/RTDS co-simulation platform is also developed to establish the bidirectional real-time communication between the proposed algorithm and the test network running (simulation) in real-time. The PQDEs are forced to occur in the network and the captured PQ signals are passed through the proposed algorithm to classify and visualize PQ disturbances in real-time.

Real Time Digital Simulator (RTDS) is a digital simulation tool, which is designed to perform real time (with typical time step of 25-50 µs) Electromagnetic Transient (EMT) simulation of complex power system. Detailed transient features of EMT phenomena, which is encountered in real power system, are captured accurately in real time by RTDS simulation. RTDS has specific hardware mounted in individual racks. The specific hardware includes several digital signal processors (DSPs) to conduct parallel processing with high speed [32]. The microgrid test system, shown in Fig. 6, is built in DRAFT module of RSCAD software through a graphical user interface (GUI).

Various PQDEs are simulated and the voltage and/or current signals are passed through the proposed algorithm coded in MATLAB running on a computer (see Fig. 7). The signals are sampled at 60×128 Hz.

Fig. 6 shows a microgrid equipped with three DERs (Distributed Energy Resources), namely, a PV (Photovoltaic) generation system, a diesel generator, and a doubly-fed induction generator (DFIG)-based wind energy system [33]. The PV and DFIG sources are connected to the AC grid through the switched VSC (voltage source converter) models controlled by sinusoidal pulse width modulation technique. The parameters of the test network are detailed in Table VII.

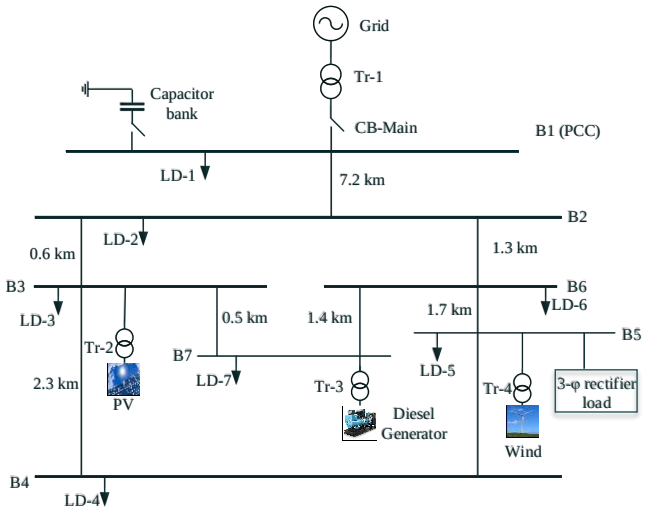

Fig. 6. Single line diagram of a test system used for the real-time simulation study on RTDS platform.

TABLE VII
Microgrid Network Parameters

Network components	Network parameters
Grid	Rated short-circuit MVA =1200, rated kV = 138, f = 60 Hz, Base voltage = 138 kV
Transformers	Tr-1: Rated MVA =25, kV =138/13.2, f = 60 Hz, X_1 = 0.08 pu, Tr-2 & Tr-4: Rated MVA= 2.5, kV=13.2/0.69, f = 60 Hz, R_1 & R_2= 0.001 pu, X_1 & X_2 = 0.1 pu, Tr-3: Rated MVA =5.5, kV =13.2/4, f = 60 Hz, X_1 = 0.1 pu.
Diesel Generator	Rated MVA = 5.5, rated kV = 4, f = 60 Hz, inertia const. (H) = 3.03, X_a = 0.13 pu, R_a = 0.002 pu, X_d = 1.79 pu, X_d' = 0.169 pu, X_d'' = 0.135 pu, X_q = 1.71 pu, X_q' = 0.228 pu, X_q'' = 0.2 pu, T_{d0}' = 4.3 s, T_{d0}'' = 0.032 s, T_{q0}' = 0.85 s, T_{q0}'' = 0.05 s.
Photovoltaic Generator (PV)	Rated MW = 1.74, rated kV = 0.69, f = 60 Hz, V_{dc} = 2500 V, No. of cells in series per module =36, No. of modules in series: 115, No. of modules in parallel: 285
Wind Energy System	DFIG parameters: rated MW = 2, f = 60 Hz, pf = 0.9, rated kV = 0.69, X_s = 0.102 pu, R_s = 0.00462 pu, X_m = 4.348 pu.
Distribution lines	π-section, V_{base} = 13.2 kV, R_1 = 1.24 Ω, R_0 = 2.52 Ω, X_{L1} = 3.1 Ω, X_{L0} = 12.95 Ω, X_{C1} = 0.036 MΩ, X_{C0} = 0.088 MΩ.
Loads	A total load of 7.5 MW+j2.8 MVAR is distributed inside the microgrid; capacitor bank: Q_c = 0.5 MVAR

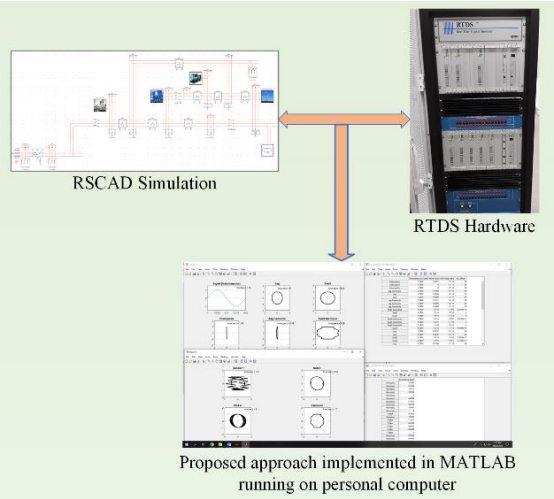

Fig. 7. Real-Time Digital Simulator (RTDS) test platform for validation of proposed approach.

A transient event is simulated by switching the capacitor bank connected at bus-1 (B1) of the test system shown in Fig. 6. The time-domain voltage or PQ signal, captured from bus-1, is shown in Fig. 8(a). The capacitor bank is switched at 0.2 sec. The event is successfully classified by the proposed algorithm as illustrated in Fig. 8(b). Fig. 8(b) exhibits a snapshot of real-time classification results demonstrated through four blocks. The title of each block specifies the classified event and the "time (sec)" placed on top right corner indicates the detection time-stamp. The PQ signal of Fig. 8(a) is classified as transient event and hence, the corresponding SVEs reside in transient block of Fig. 8(b). Moreover, from the "time (sec)" value shown in the Transient block, it is evident that the event is detected at 0.2167 sec, i.e., one cycle after the event's inception.

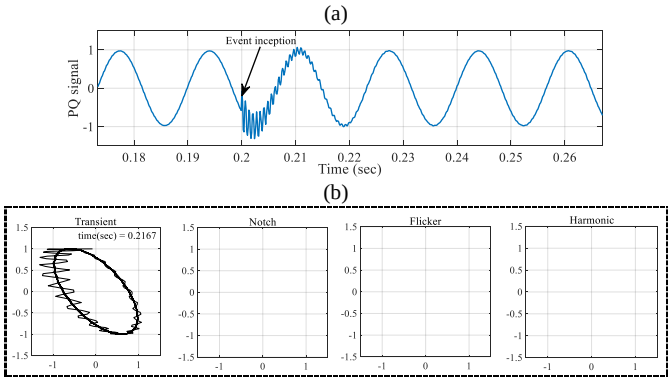

Fig. 8. (a) PQ disturbance signal due to capacitor switching, (b) shape of SVE classified as "Transient" event in real-time with detection timestamp.

Fig. 9 shows another example of PQDE and its classification results. A single line-to-ground (SLG) fault, with a duration of 7-cycle, is simulated to occur at bus-2 (B2) of Fig. 6. The voltage signal of Fig. 9(a) is collected from bus-5 (B5), adjacent to 3-phase bridge rectifier load. The snapshot of real-time classification results can be seen from Fig. 9(b), where nine blocks, entitled with the name of PQ events, exhibit different SVEs for different PQ events and their detection time in sec. The log reports of Fig. 9(c) demonstrate the detailed classification results with detection time-stamp. Sag-harmonic events are detected for the first 2-cycles, followed by sag events in the next 4-cycles and then, sag-harmonic is detected on the seventh cycle. Moreover, the severity of sags can also be realized from the semi-minor axis parameters. During the clearance of fault, a transient event is observed at 0.3167 sec, which is classified and detected at 0.333 sec, see last row of the log report of Fig. 9(c).

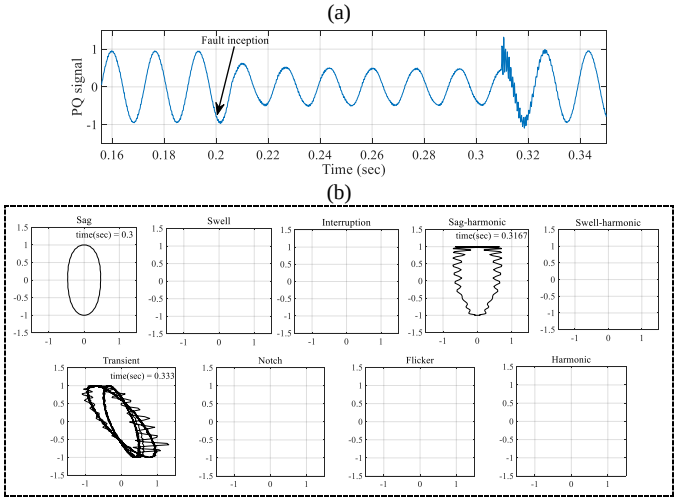

(c)

LOG REPORT OF PQ EVENTS

	Timestamp (sec)	semi-minor axis	semi-major axis	Inc_angle
sag-harmonic	0.2167	0.7463	1.0038	90
sag-harmonic	0.2333	0.5056	1.0038	90
sag	0.2500	0.5036	1.0038	90
sag	0.2667	0.4951	1.0038	90
sag	0.2833	0.4878	1.0038	90
sag	0.3000	0.4837	1.0038	90
sag-harmonic	0.3167	0.6087	1.0038	90
Transient	0.3330			

Fig. 9. (a) PQ disturbance signal due to Single line-to-ground (SLG) fault, (b) shape of SVEs classified as "Sag", Sag-harmonic", and "Transient" events in real-time with detection timestamp, (c) log report of PQ Events.

The occurrence of islanding in a microgrid is a common incident, where upstream grid disengages from an active distribution system and only distributed generators (DGs) have to feed the local loads at that instant. Hence, DGs may be over/under-loaded, which results in deviations of voltage and frequency from the nominal value of the system. One such islanding event is created at 0.26 sec by opening the main circuit breaker (CB-main) of Fig. 6. Despite the deviations from fundamental frequency during islanding, the post-islanding voltage sags are successfully classified and detected by the proposed algorithm and the results are illustrated in Fig 10. The shape of SVEs during voltage sags are shown in "sag" entitled block of Fig. 10(b). The log report of Fig. 10(c) shows the detailed classification results with detection time-stamp. Moreover, the semi-minor axis parameters reflect the severity of voltage sags.

Lastly, other PQDEs, such as notch, swell, swell-harmonic, interruption, etc., events are also simulated by changing different parameters of the test system developed in RSCAD/RTDS platform. For example, notch event is created by controlling the bridge rectifier load with different firing angles, interruption is generated by triggering a balanced/symmetrical fault at bus-2 (B2). The PQ signals associated with these PQDEs are processed through the proposed algorithm and then, they are accurately classified.

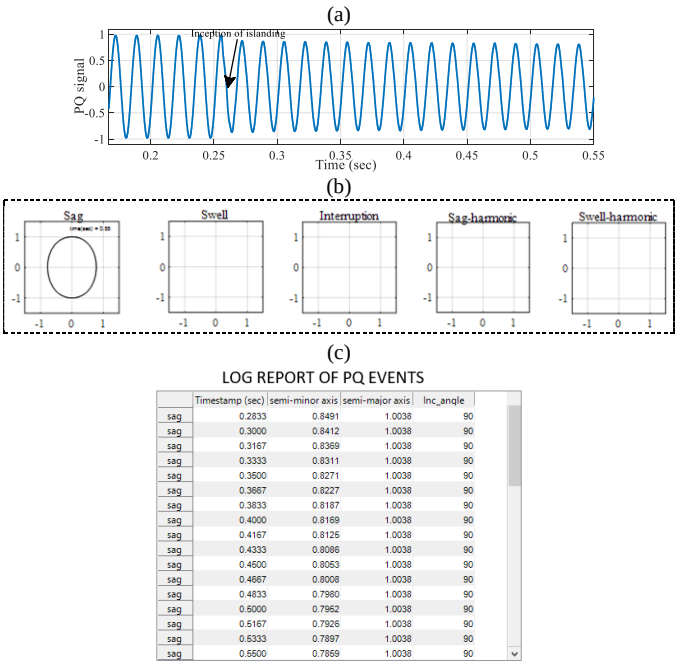

Fig. 10. (a) PQ disturbance signal due to islanding incident, (b) shape of SVEs classified as "Sag" event in real-time with detection timestamp, (c) log report of PQ events.

V. Conclusion

This paper presents a new automated approach employing space vector ellipses (SVEs) in a complex plane to detect, classify and visualize single and mixed power quality disturbance-events (PQDEs), namely, voltage sag, swell, harmonic, interruption, sag-harmonic, swell-harmonic, notch, flicker and oscillatory transient. Exploiting the ellipse parameters, our proposed algorithm allows cycle-by-cycle classification of PQ signals, thereby ensuring real-time detection of PQDEs. The validation of the proposed method is carried out using synthetic data simulated from a set of representative equations of PQ events. The robustness of the method is further tested by adding noise with synthetic data. Moreover, real data collected from the database of IEEE 1159.2 working group and EPRI are tested to assess the performance. Simulation of a microgrid test system on RTDS platform shows the credibility of proposed approach in detecting, classifying and visualizing PQDEs in real time. Various test results demonstrate the effectiveness of proposed approach and hence, it could be implemented as a potential tool for classification and visualization of PQ disturbance-events.

VI. References

[1] *IEEE Recommended Practice for Monitoring Electric Power Quality*, IEEE Std. 1159-2009, Jun. 2009.

[2] T. Chakravorti, R. K. Patnaik and P. K. Dash, "Detection and classification of islanding and power quality disturbances in microgrid using hybrid signal processing and data mining techniques," in *IET Signal Processing*, vol. 12, no. 1, pp. 82-94, 2018.

[3] *Voltage Characteristics of Electricity Supplied by Public Distribution Systems*, EN Std. 50160, 1999.

[4] H. Imtiaz and T. F. Sanam, "Frequency domain feature extraction for power quality disturbance classification," *2013 International Conference on Informatics, Electronics and Vision (ICIEV)*, Dhaka, 2013, pp. 1-5.

[5] L. Coppola, Q. Liu, S. Buso, D. Boroyevich and A. Bell, "Wavelet Transform as an Alternative to the Short-Time Fourier Transform for the Study of Conducted Noise in Power Electronics," in *IEEE Transactions on Industrial Electronics*, vol. 55, no. 2, pp. 880-887, Feb. 2008.

[6] B. K. Panigrahi and V. R. Pandi, "Optimal feature selection for classification of power quality disturbances using wavelet packet-based fuzzy k-nearest neighbour algorithm," in *IET Generation, Transmission & Distribution*, vol. 3, no. 3, pp. 296-306, March 2009.

[7] F. B. Costa, "Boundary Wavelet Coefficients for Real-Time Detection of Transients Induced by Faults and Power-Quality Disturbances," in *IEEE Trans. on Power Del.*, vol. 29, no. 6, pp. 2674-2687, Dec. 2014.

[8] K. Thirumala, A. C. Umarikar and T. Jain, "Estimation of Single-Phase and Three-Phase Power-Quality Indices Using Empirical Wavelet Transform," in *IEEE Transactions on Power Delivery*, vol. 30, no. 1, pp. 445-454, Feb. 2015.

[9] F. Hafiz, A. Swain, C. Naik, S. Abecrombie and A. Eaton, "Identification of power quality events: selection of optimum base wavelet and machine learning algorithm," in *IET Science, Measurement & Technology*, vol. 13, no. 2, pp. 260-271, 3 2019.

[10] S. M. A. Bhuiyan, J. Khan and G. Murphy, "WPD for Detecting Disturbances in Presence of Noise in Smart Grid for PQ Monitoring," in *IEEE Trans. on Ind. Applications*, vol. 54, no. 1, pp. 702-711, Jan.-Feb. 2018.

[11] M. K. Jena, B. K. Panigrahi and S. R. Samantaray, "A New Approach to Power System Disturbance Assessment Using Wide-Area Postdisturbance Records," in *IEEE Transactions on Industrial Informatics*, vol. 14, no. 3, pp. 1253-1261, March 2018.

[12] N. Senroy, S. Suryanarayanan and P. F. Ribeiro, "An Improved Hilbert–Huang Method for Analysis of Time-Varying Waveforms in Power Quality," in *IEEE Transactions on Power Systems*, vol. 22, no. 4, pp. 1843-1850, Nov. 2007.

[13] R. Kumar, B. Singh, D. T. Shahani, A. Chandra and K. Al-Haddad, "Recognition of Power-Quality Disturbances Using S-Transform-Based ANN Classifier and Rule-Based Decision Tree," in *IEEE Transactions on Industry Applications*, vol. 51, no. 2, pp. 1249-1258, March-April 2015.

[14] S. Mishra, C. N. Bhende and B. K. Panigrahi, "Detection and Classification of Power Quality Disturbances Using S-Transform and Probabilistic Neural Network," in *IEEE Transactions on Power Delivery*, vol. 23, no. 1, pp. 280-287, Jan. 2008.

[15] P. Janik and T. Lobos, "Automated classification of power-quality disturbances using SVM and RBF networks," in *IEEE Transactions on Power Delivery*, vol. 21, no. 3, pp. 1663-1669, July 2006.

[16] Z. Liu, Y. Cui and W. Li, "A Classification Method for Complex Power Quality Disturbances Using EEMD and Rank Wavelet SVM," in *IEEE Transactions on Smart Grid*, vol. 6, no. 4, pp. 1678-1685, July 2015.

[17] Chetan B. Khadse, Madhuri A. Chaudhari and Vijay B. Borghate, "Conjugate gradient back-propagation based artificial neural network for real time power quality assessment," in *International Journal of Electrical Power & Energy Systems*, vol. 82, pp. 197-206, 2016.

[18] A. M. Gaouda, S. H. Kanoun, M. M. A. Salama and A. Y. Chikhani, "Pattern recognition applications for power system disturbance classification," in *IEEE Trans. on Power Del.*, vol. 17, no. 3, pp. 677-683, July 2002.

[19] T. Zhong, S. Zhang, G. Cai and N. Huang, "Power-quality disturbance recognition based on time-frequency analysis and decision tree," in *IET Generation, Transmission & Distribution*, vol. 12, no. 18, pp. 4153-4162, Oct. 2018.

[20] M. Babakmehr, H. Sartipizadeh and M. G. Simões, "Compressive Informative Sparse Representation-Based Power Quality Events Classification," in *IEEE Transactions on Industrial Informatics*, vol. 16, no. 2, pp. 909-921, Feb. 2020.

[21] M. R. Alam, K. M. Muttaqi, and A. Bouzerdoum, "Characterizing voltage sags and swells using three-phase voltage ellipse parameters," in *IEEE Trans. on Industry Applications*, vol. 51, no. 4, pp. 2780–2790, Jul. 2015.

[22] V. Ignatova, P. Granjon, and S. Bacha, "Space vector method for voltage dips and swells analysis," in *IEEE Trans. Power Del.*, vol. 24, no. 4, pp. 2054–2061, Oct. 2009.

[23] J. R. Camarillo-Peñaranda and G. Ramos, "Fault Classification and Voltage Sag Parameter Computation Using Voltage Ellipses," in *IEEE Trans. on Industry Applications*, vol. 55, no. 1, pp. 92-97, Jan.-Feb. 2019.

[24] E. Collett, *Polarized Light in Fiber Optics*. Long Branch, NJ, USA: PolaWave Group, 2003.

[25] Thyagarajan, K. S., *Introduction to digital signal processing using MATLAB with application to digital communications*. Springer, 2019.

[26] M. Valtierra-Rodriguez, R. de Jesus Romero-Troncoso, R. A. Osornio-Rios and A. Garcia-Perez, "Detection and Classification of Single and Combined Power Quality Disturbances Using Neural Networks," in *IEEE Transactions on Industrial Electronics*, vol. 61, no. 5, pp. 2473-2482, May 2014.

[27] S. He, K. Li and M. Zhang, "A Real-Time Power Quality Disturbances Classification Using Hybrid Method Based on S-Transform and Dynamics," in *IEEE Transactions on Instrumentation and Measurement*, vol. 62, no. 9, pp. 2465-2475, Sept. 2013.

[28] M. Biswal and P. K. Dash, "Measurement and Classification of Simultaneous Power Signal Patterns With an S-Transform Variant and Fuzzy Decision Tree," in *IEEE Transactions on Industrial Informatics*, vol. 9, no. 4, pp. 1819-1827, Nov. 2013.

[29] M. A. S. Masoum, S. Jamali and N. Ghaffarzadeh, "Detection and classification of power quality disturbances using discrete wavelet transform and wavelet networks," in *IET Science, Measurement & Technology*, vol. 4, no. 4, pp. 193-205, July 2010.

[30] IEEE 1159.2 Working Group, Test Waveforms. [Online]. Available: grouper.ieee.org/groups/1159/2/testwave.html

[31] "DOE Disturbance Library," US Dept. Energy Electr. Power Res. Inst., Orlando, FL, USA. [Online]. Available: http://pqmon.epri.com/disturbance_library/see_all.asp

[32] R. Kuffel, J. Giesbrecht, T. Maguire, R. P. Wierckx, and P. McLaren, "RTDS-A fully digital power system simulator operating in real time," in *Proc. IEEE WESCANEX Commun. Power Comput. Conf.*, vol.2. Winnipeg, MB, Canada, 1995, pp. 300-305.

[33] O. Nzimako and A. Rajapakse, "Real time simulation of a microgrid with multiple distributed energy resources, " in *Proc. 2016 International Conference on Cogeneration, Small Power Plants and District Energy (ICUE)*, Bangkok, 2016, pp. 1-6.